



HAL
open science

On the modelling of wavepacket scattering noise with coherence effects

Filipe da Silva, Peter Jordan, André Cavalieri

► **To cite this version:**

Filipe da Silva, Peter Jordan, André Cavalieri. On the modelling of wavepacket scattering noise with coherence effects. *Journal of the Acoustical Society of America*, 2019, 146 (6), 10.1121/1.5140190 . hal-02380357

HAL Id: hal-02380357

<https://hal.science/hal-02380357>

Submitted on 26 Nov 2019

HAL is a multi-disciplinary open access archive for the deposit and dissemination of scientific research documents, whether they are published or not. The documents may come from teaching and research institutions in France or abroad, or from public or private research centers.

L'archive ouverte pluridisciplinaire **HAL**, est destinée au dépôt et à la diffusion de documents scientifiques de niveau recherche, publiés ou non, émanant des établissements d'enseignement et de recherche français ou étrangers, des laboratoires publics ou privés.

On the modelling of wavepacket scattering noise with coherence effects

Filipe D. da Silva,¹ Peter Jordan,² and André V. G. Cavalieri³

¹*Departamento de Engenharias da Mobilidade, Universidade Federal de Santa Catarina, Joinville-SC, 89219-600, Brazil*

²*PPRIME Institute, CNRS - ENSMA - Univ. Poitiers, Poitiers, 86036, France*

³*Instituto Tecnológico de Aeronáutica, São José dos Campos, 12228-900, Brazil*

(Dated: 22 September 2019)

1 An investigation of a wavepacket model for free-jet and jet-surface interaction noise
2 was conducted. The source term for the axisymmetric mode was extracted from a
3 Mach 0.9 jet Large Eddy Simulation (LES) and employed to adjust the parameters
4 of a simple source model. Streamwise coherence decay, in particular, was considered.
5 The source model was propagated with both the free-field and tailored Green's func-
6 tion for a semi-infinite flat plate positioned at a distance of $r/D = 1$ from the jet
7 axis. First, a model with radial content was considered. Significant deviations were
8 observed in the prediction of the low-angle directivity of the isolated jet as well as
9 in the reproduction of the characteristics of the source field. However, the effects
10 of trailing edge noise were well reproduced. The installed jet case, (~~Added: at the~~
11 ~~region dominated by trailing-edge scattering~~), showed very little sensitivity to the co-
12 herence decay, a crucial feature in the isolated jet case. (~~Deleted: Through the use~~
13 ~~of a line source, involving greater ease in the adjustments, the models were capable to~~
14 ~~predict the acoustic fields in all studied configurations in low Strouhal number.~~) The
15 modelling of installed jets proved to be much simpler, since the results were much
16 less sensitive to the characteristics of the source.

^{a)} filipe.dutra@ufsc.br; Corresponding author.

17 I. INTRODUCTION

18 The adverse effects arising from the integration of engines with the aircraft structure have
19 gained importance with the rise of stricter noise regulations. Among the sources of noise
20 due to this integration are the interaction of the jet flow with wings and flaps. In this case
21 the problem is intensified by the close coupling between the engine and the wing, due to the
22 use of high bypass ratio engines.

23 The effects caused by the presence of solid surfaces near turbulent regions have been
24 known for decades. Curle¹ presented an extension of Lighthill's theory² in order to account
25 for the influence of solid boundaries on the acoustic field. In addition to the jet quadrupoles,
26 surface pressure leads to the appearance of dipole sources, which have stronger far-field
27 contribution at low Mach numbers. Furthermore, Ffowcs Williams and Hall³ studied the
28 case involving semi-infinite plates using a tailored Green's function. In this case, the deduced
29 edge scattering source is even more efficient than both the free turbulence in Lighthill's
30 theory or compact surfaces in Curle's work.

31 Wavepackets are intermittent, advecting disturbances that are correlated over distances
32 far exceeding the integral scales of turbulence⁴. Several experimental and theoretical studies
33 highlighted the importance of such structures in jet noise⁵⁻⁸. Theoretical models based on
34 wavepackets have been shown to capture many of the main characteristics of the far-field
35 noise for isolated^{8,9} and installed jet cases¹⁰⁻¹². However, inconsistencies are present as the
36 absolute noise levels are under predicted by linear dynamic models, such as the Parabolised
37 Stability Equations. These linear models have unit coherence in contrast with turbulent

38 flows, in which coherence decays with distance. This issue was investigated by Cavalieri and
39 Agarwal¹³ who show the match of the coherence of the original source to be fundamental
40 for correctly predicting the sound field. Studies showed that the coherence decay found
41 in turbulent jets, when included in the linear models, raise the radiating efficiency of the
42 source¹³⁻¹⁵.

43 Regarding installation effects, Cavalieri *et al.*¹⁰ modelled a jet-plate interaction case using
44 a wavepacket source model along with a tailored Green's function and a boundary element
45 method. The scattering of the non-compact wavepackets in the jet near field was found to
46 be responsible for the amplification of the noise due to the presence of the plate. The used
47 model was identified from far-field measurements of free jet noise. Further studies are needed
48 to evaluate the pertinence of the model, and it would be important to use data from jet
49 turbulence to construct a source. Moreover the role of jitter/coherence decay is apparently
50 weaker in installed jet noise according to Nogueira *et al.*¹², but the cited work dealt with a
51 model problem. Again, the use of turbulence data may help addressing this question in a
52 more definite way. (Added: The use of model sources and Lighthill's equation for predicting
53 installed jet noise has been also explored by Refs. 16, 17 and 18.)

54 The objective of this paper is to analyse wavepacket source models, obtained from nu-
55 merical flow data, for the prediction of free-jet and jet-plate interaction noise. We first
56 investigate simplifications on the Lighthill's source term and their relevance to the total
57 sound field using the LES data from Ref. 19. Subsequently, the same numerical data is used
58 to obtain parameters of kinematic wavepacket source models, and the produced noise field

59 was obtained using both the free-field Green’s function and a tailored Green’s function for
 60 a semi-infinite flat plate.

61 This work is organized as follows. In section II, we describe the used geometries and the
 62 main equations. In section III, we present the acoustic results from a simplified source term
 63 extracted from the LES data. Results for the model source are presented in section IV.
 64 Finally, section V presents the main conclusions.

65 II. METHODS

66 A. Geometry

67 The study presented herein is based on the experiments conducted at PPRIME Institute,
 68 Poitiers, France¹¹. The experiment consists of a nozzle of diameter $D = 50$ mm with a flat
 69 plate positioned at its vicinity, as shown in the sketch of Fig. 1. (Added: The plate has a
 70 chord of $9D$ and a span length of $15D$.) A total of 324 acoustic field measurements were
 71 taken on a cylindrical surface of radius $R = 14.2D$. The studied configuration had a jet
 72 acoustic Mach number $M_a = 0.9$ and Reynolds number $Re_j = \rho_j U_j D / \mu_j \approx 1 \times 10^6$. The
 73 trailing-edge position at the center of the plate is $x/D = 4$ and $r/D = 1$ is the position
 74 relative to the nozzle axis; here we consider a cylindrical coordinate system, with origin
 75 at the nozzle exit, given by (x, r, ϕ) , corresponding to streamwise, radial and azimuthal
 76 coordinates, respectively.

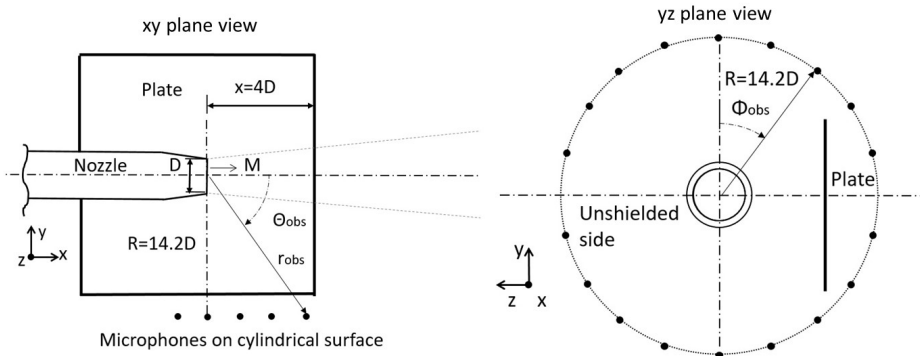


FIG. 1. Scheme of the experimental tests used as reference in this analysis.

77 B. Large eddy simulation database

78 The large eddy simulation (LES) database used corresponds to the same jet conditions
 79 and nozzle geometry, considering only the free-jet case. (Added: The jet is isothermal in
 80 the simulation.) The simulation was performed using the compressible flow solver “Charles”
 81 developed at Cascade Technologies, and reproduces the configuration from the companion
 82 experiment conducted at the PPRIME Institute, Poitiers, France.

83 The LES methodology, grid resolution study and validation with experiments are pre-
 84 sented in details in Brès *et al.*¹⁹. The instantaneous values of the primitives variables were
 85 interpolated from the original unstructured LES grid onto structured cylindrical grids in the
 86 jet plume and in the nozzle pipe. These cylindrical grids were designed such that the reso-
 87 lution approximately corresponds to the underlying LES resolution. For the jet plume, the
 88 cylindrical grid extends to $0 \leq x/D \leq 30$, $0 \leq r/D \leq 6$, with $(n_x, n_r, n_\phi) = (626, 138, 128)$,
 89 where n_x , n_r and n_ϕ are the number of points in the streamwise, radial and azimuthal direc-
 90 tion, respectively. The points are equally-spaced in the azimuthal direction to enable simple
 91 azimuthal decomposition in Fourier space.

92 **C. Eduction of the source term from LES**

93 The source term is based on the Lighthill² equation given by,

$$\frac{\partial^2 \rho}{\partial t^2} - c^2 \nabla^2 \rho = \frac{\partial^2 T_{ij}}{\partial x_i \partial x_j}, \quad (1)$$

94 where the Lighthill's tensor, with viscous terms neglected, is defined as, $T_{ij} = \rho U_i U_j + (p -$
 95 $c^2 \rho) \delta_{ij}$, where U_i is the velocity vector, p the pressure, ρ the fluid density, c the speed of
 96 sound and δ_{ij} the Kronecker delta.

97 We now apply several simplifications to the source term, which nonetheless are expected to
 98 retain the main source features for sound generation^{8,14}. The entropy term is not considered
 99 for an isothermal jet and source density variations are substituted by the mean ρ_0 . Under the
 100 hypothesis of the predominance of the momentum term T_{xx} , separating mean and fluctuating
 101 parts of the streamwise velocity $U_x = \overline{U_x} + u_x$ and taking only the linear part, the source
 102 term in cylindrical coordinates is given by:

$$S^t = \frac{\partial^2 T_{xx}}{\partial x^2} = \rho_0 \frac{\partial^2}{\partial x^2} 2\overline{U_x} u_x(x, r, \phi, t). \quad (2)$$

103 The source is decomposed into azimuthal Fourier modes, as we are interest in just the
 104 axissymmetric component:

$$S^t(x, r, m, t) = \frac{1}{2\pi} \int_{-\pi}^{\pi} S^t(x, r, \phi, t) e^{im\phi} d\phi, \quad (3)$$

105 and only $m = 0$ is considered,

$$S^t = \frac{\partial^2 T_{xx}}{\partial x^2} = \rho_0 \frac{\partial^2}{\partial x^2} 2\overline{U_x} u_x(x, r, m = 0, t). \quad (4)$$

106 (Added: By neglecting T_{rr} and T_{xr} radiation is expected to be predominant towards low
 107 angles²². Also, non-linear terms should be significant only at sideline angles as studied by
 108 Freund⁷. Furthermore, mode 0 is expected to be dominant at at polar angles close to 30°,
 109 while the contributions of modes 1 and 2 are more significant at high angles^{8,24}.)

110 The superscript t implies the quantities in the time domain. This source term is Fourier
 111 transformed with using the following convention

$$S = \int_{-\infty}^{\infty} S^t e^{-i\omega t} dt. \quad (5)$$

112 The source distribution is obtained from the LES database, which is for a free jet. It
 113 will be used in calculations of free and installed jet noise, as will be presented in the next
 114 sections. For the installed jet calculations, there is an implicit assumption that the presence
 115 of a neighbouring plate does not modify substantially the source field. The accuracy of the
 116 calculation may serve as an *a posteriori* check of this assumption.

117 **D. Computation of the acoustic pressure at observer positions**

118 The source distribution obtained from the LES database, with the simplifications de-
 119 scribed in the previous section, allow an estimation of the radiated sound in free- and
 120 installed-jet configurations. The calculation is done in the frequency domain, based on
 121 the integral solution of the inhomogeneous Helmholtz equation, resulting from the Fourier

122 transform of Lighthill's equation. As we are dealing with turbulent properties, and so non
 123 square-integrable functions, it is more appropriate to work with two-point statistics. In this
 124 sense, the Power Spectral Density (PSD) of the sound pressure field can be obtained from
 125 the Cross Spectral Density (CSD) of the source field by:

$$\begin{aligned}
 \langle p(\mathbf{x}, m, \omega) p^*(\mathbf{x}, m, \omega) \rangle = & \\
 \int_V \int_V \langle S(\mathbf{y}, m, \omega) S^*(\mathbf{z}, m, \omega) \rangle G(\mathbf{x}, \mathbf{y}, \omega) G^*(\mathbf{x}, \mathbf{z}, \omega) d\mathbf{y} d\mathbf{z} & \quad (6)
 \end{aligned}$$

126 For the free jet case, $G = G_0$ is the free-field Green's function given as,

$$G_0 = \frac{e^{-ikR}}{4\pi R} \quad (7)$$

127 where R is the distance between source and observer and $k = \omega/c_0$ the acoustic wavenumber.

128 For the installed jet case, the problem is modelled as the jet scattering from a semi-
 129 infinite plate. This approach has been used with wavepacket models and was shown to be
 130 representative of the problem, although some deviations occur due to the differences to the
 131 real case (finite plate)¹⁰⁻¹². The tailored Green's function from Ffowcs Williams and Hall³
 132 is used,

$$4\pi G_t = \frac{e^{\frac{1}{4}i\pi}}{\sqrt{\pi}} \left\{ \frac{e^{-iR}}{R} \int_{-\infty}^{u_R} e^{-iu^2} du + \frac{e^{-iR'}}{R'} \int_{-\infty}^{u_{R'}} e^{-iu^2} du \right\} \quad (8)$$

133 where,

$$U_R = 2 \left(\frac{kr r_0}{D + R} \right)^{\frac{1}{2}} \cos \frac{\theta - \theta_0}{2}, \quad (9)$$

$$u_{R'} = 2 \left(\frac{krr_0}{D + R'} \right)^{\frac{1}{2}} \cos \frac{\theta + \theta_0}{2}, \quad (10)$$

$$D = \{(r - r_0)^2 + (z - z_0)^2\}^{\frac{1}{2}}. \quad (11)$$

134 The tailored Green's function on its original form, implies a cylindrical coordinate system
 135 with axial coordinate aligned with the trailing edge. The position of the source point in this
 136 coordinate system is (r_0, θ_0, z_0) and the observer (r, θ, z) . R is then the distance between
 137 source and observer and R' is the distance between the source's image and observer.

138 As numerical derivatives of the turbulent data generated undesirable noise in the results,
 139 the derivatives were transferred to the Green's function. The derivatives were performed
 140 analytically and the derivation from Nogueira *et al.*¹² is used for the tailored Green's function.

141 The whole available LES time data was used, with a total non-dimensional time of
 142 $tc_0/D = 2000$ and a sampling rate of $\Delta tc_0/D = 0.2$. (Added: The source domain extended
 143 $0 \leq x/D \leq 30$, $0 \leq r/D \leq 3$, with $(n_x, n_r) = (328, 58)$ points.) The Cross Spectral Densi-
 144 ties (CSDs) were calculated using Welch's method²⁰ using block size of Nfft= 256 timesteps,
 145 overlap of 75%. Sensitivity tests for the window function were conducted. Acoustics re-
 146 sults obtained from the CSD calculated with rectangular window presented an undesirable
 147 dependence with the block size. Nevertheless, results with Hanning window showed much
 148 lower sensitivity to the block size. Based on these results, the Hanning window was chosen
 149 for further analyses.

150 **E. Model sources**

151 Model sources used in this work are inspired by the wavepacket line source model pre-
 152 sented by Crow²¹ (see Crighton²²). This source and variations were used in Refs. 8, 10–12,
 153 some of them introducing radial information with the insertion of radial profiles obtained
 154 via PSE solutions. Based on the coherence modelling proposed by Cavalieri and Agarwal¹³
 155 the following source model is employed:

$$\begin{aligned} \langle S(\mathbf{x}_1, \omega) S^*(\mathbf{x}_2, \omega) \rangle = & A \exp \left(-\frac{(x_1 - X_c)^2}{L_x^2} - \frac{(x_2 - X_c)^2}{L_x^2} \right) \\ & \operatorname{erfc} \left(\frac{\alpha(x_1 - X_c)}{\sqrt{2}L_x} \right) \operatorname{erfc} \left(\frac{\alpha(x_2 - X_c)}{\sqrt{2}L_x} \right) \exp \left(-\frac{(r_1 - R_c)^2}{L_r^2} - \frac{(r_2 - R_c)^2}{L_r^2} \right) \\ & \exp [-ik_h(x_1 - x_2)] \exp \left(-\frac{|\mathbf{x}_1 - \mathbf{x}_2|^2}{L_c^2} \right), \end{aligned} \quad (12)$$

156 such that the *CSD* of the source is represented by 7 global parameters. A represents the
 157 maximum *PSD* amplitude, whose streamwise decay is represented by an asymmetric Gaus-
 158 sian profile centered at X_c with characteristic length L_x and α as the skewness parameter.
 159 The radial profile is represented by a symmetric Gaussian profile with envelope length L_r .
 160 Centering this second Gaussian at $R_c = 0.25$ was taken as a reasonable assumption. Stream-
 161 wise phase difference is defined by the hydrodynamic wavenumber k_h , related to the phase
 162 speed $U_c/U_J = 2\pi St/k_h$.

163 Finally the coherence decay is represented by Gaussian profiles of characteristic length
 164 L_c . The parameters were obtained by minimizing the sum of the squares of the absolute
 165 error between the numerical source and the proposed model.

166 ~~(Deleted: In order to further simplify the model, a line source approach, similar to Ref.~~
 167 ~~13 is derived. For a free jet case, at low St number, with observer at the far field with~~
 168 ~~$(r_{obs} \gg r_s)$ it is acceptable to assume radial compactness, leading to an independence of the~~
 169 ~~Green's function with the radial distance. In this way parting from the eq. 6 becomes,)~~

170 ~~(Deleted: with the CSD of the line source defined as)~~

171 ~~(Deleted: This line source can be parametrised in a similar manner to the volumetric~~
 172 ~~source in eq. 12, leading to)~~

173 III. SOUND RADIATION FROM LES SOURCE TERMS

174 A. Isolated jet

175 The linearised, $m = 0$, T_{xx} source term extracted from the LES was first propagated
 176 by the integration with the free-field Green's function (Eq. 6). As already known^{8,23,24}, the
 177 axisymmetric mode is dominant at low polar angles, while higher order modes are important
 178 at high angles. Only $m = 0$ experimental data is show for the free-jet case, while the complete
 179 set of azimuthal modes will be used for the installed case.

180 Results obtained by the integration with the free-field Green's function are shown in Fig. 2
 181 (LES source) for $St = 0.2, 0.3$ and 0.75 . The results show good agreement to experimental
 182 data for $m = 0$ at low angles and St numbers, reproducing the axisymmetric super directive
 183 features⁸. Although the agreement is indeed very good at $St = 0.2$ (Fig. 2(a)), levels are
 184 overpredicted at 20° and 30° for the other St .

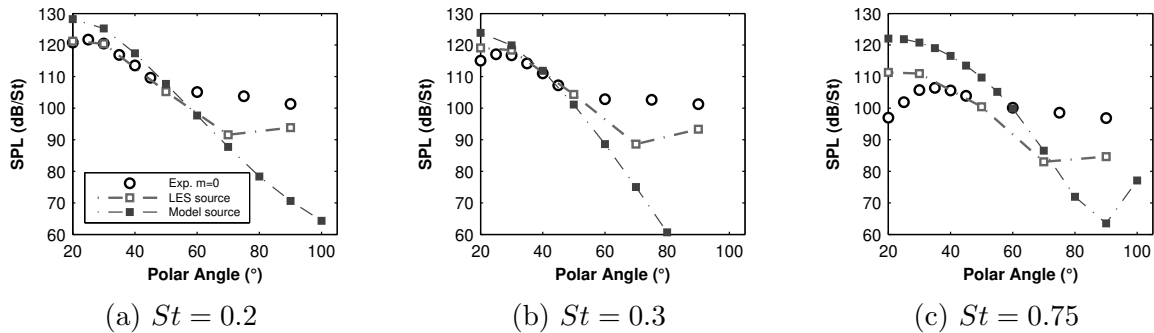


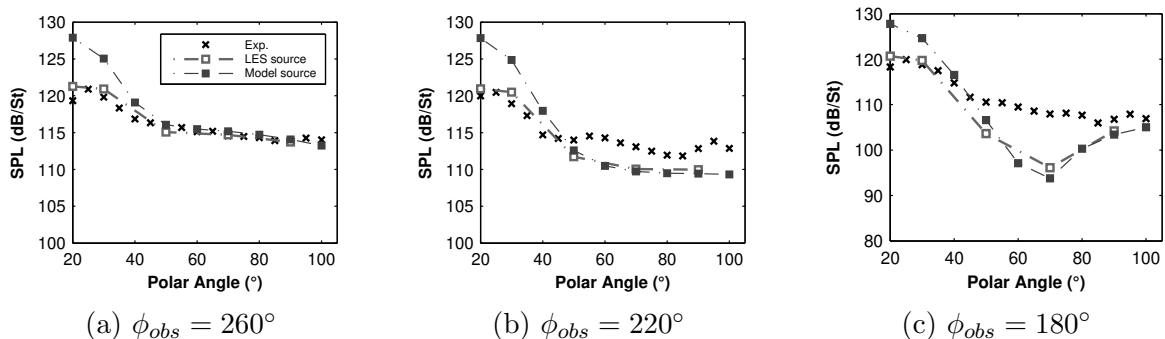
FIG. 2. Comparison of free jet results for the three considered St numbers.

185 Neglecting the entropy term in the definition of the source term could be an important
 186 issue for these observed deviations, since Bodony and Lele²⁵ identified a cancellation effect
 187 between the entropy and momentum terms for St below 0.3 at this radiation direction. How-
 188 ever, we should keep in mind that the analysed jet is isothermal, unlike the one considered
 189 in the cited study. Here, the disparities become larger with growing St , and which is also
 190 aligned with the growing importance of refraction effects. These deviations are expected to
 191 reduce once the complete Lighthill's tensor is taken into account.

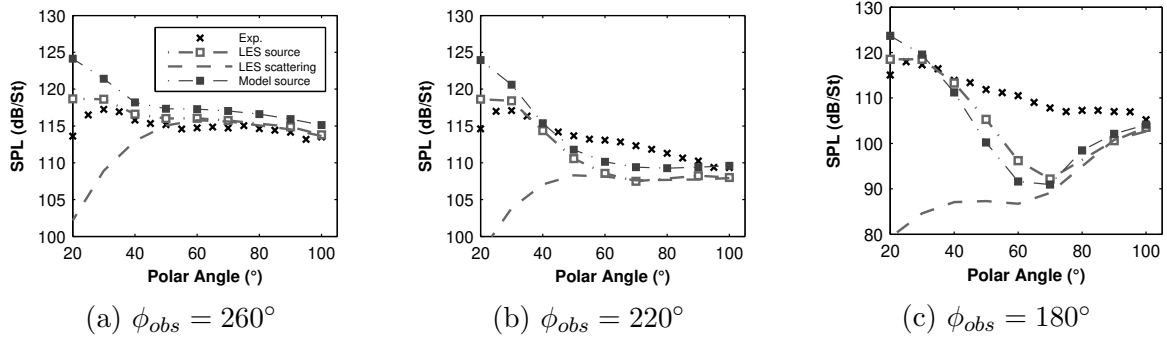
192 By looking at angles higher than 60°, we see that levels were underpredicted by about
 193 10 dB. At these directions both T_{rr} and T_{xr} and possibly non-linear terms have considerable
 194 contribution to total noise levels, but were not considered in this study²². As already ex-
 195 pected, more terms and more azimuthal Fourier modes should be accounted for when trying
 196 to predict noise at high angles for an isolated jet.

197 **B. Installed Jet, plate at $r/D = 1$**

198 Fig. 3(a) and 4(a) depict the results for the installed case (Added: (LES source)) for
 199 azimuthal angle $\phi_{obs} = 260^\circ$, at the unshielded side of the plate (See Fig. 1). For the
 200 region dominated by the edge scattering (polar angles around 90°), levels were close to the
 201 experimental total noise (all modes). This now points out to the dominance of the mode
 202 $m = 0$ and T_{xx} for installed jet noise, which is in line with the results of Refs. 10 and 12. This
 203 observation supports the study in the following section, where a simplified axisymmetric T_{xx}
 204 wavepacket model source is adjusted to predict the installation noise field. (Added: In order
 205 to evidence the contribution of the plate to the total noise, the scattered only noise field was
 206 included in the same plots.)

FIG. 3. Comparison of installed jet results for $St = 0.2$.

207 For $St = 0.2$ and 0.3 in Fig. 3(Added: b) and 4(Added: b) at $\phi_{obs} = 220^\circ$, results are
 208 underpredicted by about 2 to 4 dB. We should bear in mind that the azimuthal directivity
 209 of (Replaced: installed-jet replaced with: edge-scattering) noise is of dipole shape, peaking
 210 at $\phi = 90^\circ$ and 270° and with minima at $\phi = 0, 180^\circ$ ²⁶; thus, from $\phi = 260^\circ$ to 220° we
 211 are moving to a region of lower installation effects. Furthermore, at $M = 0.9$, (Replaced:


 FIG. 4. Comparison of installed jet results for $St = 0.3$.

212 ~~installation~~ replaced with: ~~trailing-edge~~ effects are not so prominent as in lower Mach
 213 number^{11,27}. In this sense, in such radiation direction, the free jet could present noise levels
 214 comparable to the scattered field. Thus, the remaining terms and modes in the Lighthill
 215 source have some contribution at this position. In addition, the differences between the real
 216 finite plate and its representation by the semi-infinite plate may also play a role for the
 217 observed deviations. This is supported by the presence of level oscillations with the polar
 218 angle in the experimental data, potentially caused by the secondary scattering by lateral
 219 edges¹⁰.

220 Minor scattering effects are expected in directions parallel to the trailing edge in the
 221 case of the semi-infinite plate. As consequence the results for $\phi_{obs} = 180^\circ$ (Fig. 3(c)), polar
 222 directivity trends are more similar to those observed for the free jet and so, the missing
 223 modes and momentum terms are also important.

224 IV. SOUND RADIATION FROM MODEL WAVEPACKET SOURCE

225 We now benefit from the presented LES data to adjust a simple kinematic wavepacket
 226 source model, such as the ones proposed by^{8,10,13,21}. One of the objectives here is to explore
 227 the effects of the coherence decay in the isolated and installed jet configurations. The
 228 resulting model contributes both to the understanding of the underlying physics of the
 229 problem, highlighting the relevant wavepacket parameters to predict installation effects.

230 A. Two-dimensional source model

231 The model parameters were obtained by minimising the sum, (Added: over the discretized
 232 domain,) of the squares of the absolute error between the LES source (Added: CSD) and the
 233 proposed model (Eq. 12) (Added: $(\sum^N \sum^N (||CSD_{LES} - CSD_{model}||^2))$). The domain for
 234 the fitting was limited between $x = 0.5D$ and $x = 15D$ and $r = 0.2D$ and $r = 1D$ (Added:
 235 with a total number of N points). (Added: The process is carried out with the Nelder-Mead
 236 Simplex Algorithm²⁸). The parameters found for each St are summarized in table I. The total
 237 relative error ($\Delta = \sum^N \sum^N ||CSD_{LES} - CSD_{model}|| / \sum^N \sum^N ||CSD_{LES}||$) is shown in the
 238 same table. For the noise computation, the model source was defined on a grid extending
 239 from $x = -7L_x$ to $x = 7L_x$ and from $r = 0$ to $r = 1D$, with 25 points in the radial and
 240 256 points in the axial directions. Results were verified to be grid independent with these
 241 values. Acoustic results are show in Fig. 2(a) ($St = 0.2$), Fig. 2(b) ($St = 0.3$) and Fig. 2(c)
 242 ($St = 0.75$) for the free jet.

243 Levels were overpredicted by about 7 dB for $St = 0.2$ and 4 dB for $St = 0.3$ at 20° . For all
 244 considered St , levels were highly underpredicted over 60° . The low-angle directivity for the
 245 axisymmetric mode could only be reasonably captured for $St = 0.2$. Results for $St = 0.75$
 246 reasonably reproduced the directivity trends, however, noise levels were overpredicted by
 247 about 10 dB.

248 Some deviations from the expected low-angle directivity occurred and seem to increase
 249 with St . One possible cause are fitting errors. The failure of the model on capturing the
 250 sideline noise may not be unsettling, since the axisymmetric mode and even the T_{xx} term do
 251 not have the main contributions to the total noise. However, at low angles, the difficulties in
 252 predicting both the magnitude and directivity of the sound field do represent an important
 253 issue.

254 With the plate at $r/D = 1$, at polar angles dominated by the edge scattering noise and
 255 $\phi_{obs} = 260^\circ$ (Fig. 3 and 4), levels were much closer to the reference experimental and LES
 256 data. Deviations were less than 1 dB for $St = 0.2$ and about 2.5 dB for $St = 0.3$. Trailing-
 257 edge effects are not expected to be important at $St = 0.75$ so installed results were omitted
 258 for this case.

259 In Fig. 5, we can see the comparison between experimental and model results for all the
 260 measured directivity range, with the plate at $r/D = 1$, $St = 0.3$. The directivity trends
 261 could be well captured for azimuthal angles close to the plane perpendicular to the plate,
 262 say between $\phi_{obs} = 50^\circ$ and 140° and between $\phi_{obs} = 220^\circ$ and 320° . With the results up to
 263 this point, we can note that although the wavepacket model showed some deviations in the
 264 prediction of free jet noise, specially at high angles and high St , a close match is obtained

265 wherever edge scattering is dominant. These results are aligned with the observations from
 266 section III and with Cavalieri *et al.*¹⁰.

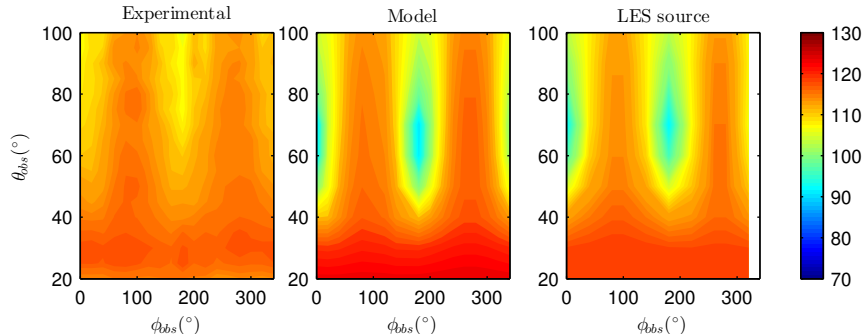


FIG. 5. (Color online) Model source SPL results compared to the experimental data with tailored Green's function at all the measured positions ($St = 0.3$).

267 We can note that the relative errors shown in table I are high, specially for $St = 0.75$,
 268 and imply a limitation of the used fit. In order to help understanding the possible causes of
 269 the found deviations, we now look at the plots of the source region. A comparison between
 270 the LES and model sources can be observed in Fig. 6 for the real part of the CSD, for each
 271 of the analysed St and for two fixed radial reference positions at $x_{ref} = X_{max}$, where X_{max} is
 272 the streamwise position of the peak power spectral density. The fitting technique provided a
 273 good representation of the maximum amplitude at $r = R_c$ and source extension around the
 274 maximum. Nevertheless, there is a clear mismatch between the radial profiles up to $x/D = 5$
 275 and in the jet shear-layer. The use of simple Gaussian profiles for the radial amplitudes and
 276 coherence contributed to these deviations, which become larger at higher St .

277 As depicted Fig. 6, at $St = 0.2$ and reference position $r_{ref} = 0.3$, the model reproduces
 278 the main characteristics of the source up between $x/D = 5$ and 10. Greater divergence can

279 be observed up to $x/D = 5$ around the lipline. When the reference point is at the lipline,
 280 the disparities are even more evident. Similar conclusions can be drawn for the other St ,
 281 with even greater disparities at $r_{ref} = 0.5D$. Deviations from the reference data seem to
 282 increase with St , as well as the sound-field results.

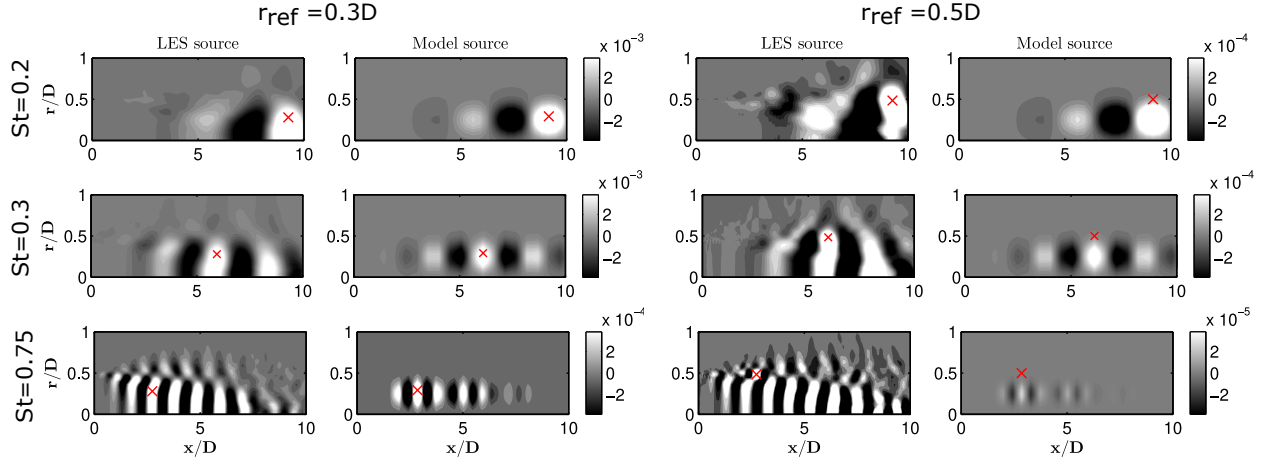


FIG. 6. Comparison between plots of real part of the CSD obtained from the LES data and from the model source with $x_{ref} = X_{max}$ at $St = 0.2$ (top), $St = 0.3$ (middle) and $St = 0.75$ (bottom).

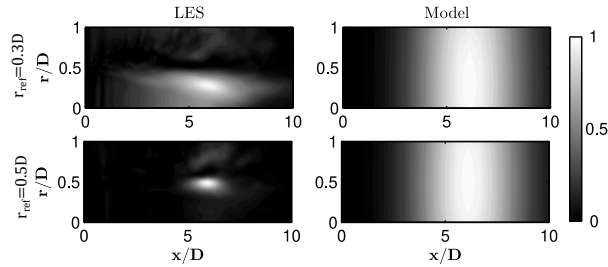


FIG. 7. Comparison between coherence plots obtained from the LES data and from the model source with $x_{ref} = X_{max}$ and $St = 0.3$ and two radial reference positions $r_{ref} = 0.3D$ (top) and $r_{ref} = 0.5D$ (bottom).

283 The comparison of coherence plots is depicted in Fig. 7 for reference points at $r/D = 0.3$
 284 and 0.5. The radial coherence decay is obviously not well reproduced by the model. At
 285 $r_{ref} = 0.3D$, the streamwise coherence could be reasonably represented. However, at $r_{ref} =$
 286 $0.5D$, a much shorter coherence length is required. This range of coherence length scales in
 287 different regions of the source field is not easy to represent with a simple kinematic model.

288 The content of the Green's functions in the wavenumber space are different^{12,13}, which
 289 would permit source wavenumbers that are evanescent in the free-field case to generate far-
 290 field noise when the jet is close to a flat plate. Slight changes in wave-packet envelope or
 291 coherence decay may influence free-jet noise substantially¹³, and lead to little changes for
 292 installed jets¹². That is possibly why the results with the plate were in good agreement with
 293 the reference data, despite of the problems observed in the free-jet case.

294 Although it is not straightforward to tell which are the causes of errors in the acoustic pre-
 295 diction by simply looking at the source field, it is evident that some considerable deviations
 296 are present between the fitted wavepacket model and the LES field. These were possibly
 297 caused by the use of simple functions for both the amplitudes and coherence, as well as by
 298 the neglect of the radial phase differences and radial coherence. However, we are working
 299 in the framework of simple kinematic models, and so a parametrisation that would be too
 300 complex is not the intention of this work. Furthermore, is important to emphasize that,
 301 even with the mentioned simplifications, the model could correctly represent the expected
 302 noise characteristics the phenomenon (Added: of trailing-edge scattering, one of the main
 303 phenomena of installed jets) (Deleted: for the installed case). Using the same 7-parameter

304 model, the next section aims at characterising the sensitivity of the results to the coherence
 305 length.

306 B. Sensitivity to the coherence length

307 As already mentioned, the coherence length is an imperative parameter in wavepacket
 308 models for isolated jet prediction^{13,15}. We now assess the effects of the variation of this
 309 parameter based on the range of values identified in the LES data at $x = X_c(St)$ and
 310 $St = 0.3$. Three values were defined: the value at the lipline ($L_c^C = 0.94$), the radial average
 311 of L_c until $r = 0.5D$ ($L_c^B = 2.66$) and the fitted value from the previous section ($L_c^A = 3$).
 312 The unit coherence source, with $L_c^0 \rightarrow \infty$, was also considered.

313 By looking at the resulting free-jet far-field noise for $St = 0.3$ in Fig. 8, we can see a clear
 314 change in the noise directivity with the different L_c values. The source with the lipline L_c
 315 produces very high noise levels in comparison with the LES source. Although reasonable
 316 level agreement at low angles was only achieved when considering the larger, original L_c ,
 317 only results with L_c^C reproduced the low-angle directivity trends. As expected^{13,15}, the L_c^0
 318 source resulted in levels at least 12 dB lower than the reference data.

319 (Added: Fig. 8 also show the results for the total noise from the jet-plate configuration.)
 320 The significant changes in level and directivity with L_c , found for the free jet, does not occur
 321 in the installed case at $\phi_{obs} = 260^\circ$, over $\theta_{obs} = 50^\circ$. In this case, the results are much less
 322 dependent on the coherence parameter, and agreement at the edge-scattering-dominated
 323 region is good even for the unit coherence source. (Added: The total noise for L_c^C for the
 324 same observer positions differs from the others by about 3 4 dB at $\theta_{obs} = 100^\circ$, however we

325 should not that these levels are very similar to those of the free-jet with the same L_c value.
 326 However, we cannot observe such differences when looking at the separated scattering field,
 327 shown in the same figure.) By looking at (Added: the total noise at) $\phi_{obs} = 220^\circ$, we can
 328 note that this sensitivity becomes higher as the observer moves to a direction parallel to
 329 the plate trailing-edge, where the scattering effects are reduced. (Added: The plots for the
 330 scattering-only noise in Fig. 8 confirms that the sensitivity is higher at $\phi_{obs} = 220^\circ$.) Indeed,
 331 the sensitivity to coherence seems to be much lower wherever edge scattering effects are
 332 dominant. Results for $St = 0.2$ showed similar trends to $St = 0.3$ and were omitted here for
 333 conciseness.

334 ~~(Deleted: One extra featured to be observed is that the installed-jet levels are very similar
 335 to the free jet for the lowest L_c^C at high angles, say above 80° . The possible reasons are
 336 that the resulting free jet noise is so high, that it masks the scattering noise and that
 337 the source is approaching the compact limit, such that scattering effects are reduced, as
 338 observed by Nogueira *et al.*¹². The main conclusion from these results is that the scattered
 339 field demonstrates low sensitivity to the coherence decay, and seems to depend more strongly
 340 on other model parameters.)~~

341 (Added: When moving the plate away from the jet, say $r/D = 1.5$, reduction of the
 342 scattering effects is expected. Fig. 8 depicts the results with the plate at at this position.
 343 Again, the sensitivity to coherence seems to be very low when edge scattering effects are
 344 dominant. As already commented the levels obtained for L_c^C are influenced by the very high
 345 free jet noise.)

346 (Added: Finally, the plate was kept at $r/D = 1$ and its trailing-edge was moved to other
 347 three axial positions ($x_{TE} = 2D$, $x_{TE} = 6D$ and $x_{TE} = 8D$). Results are shown in Fig. 10 for
 348 $\phi_{obs} = 260^\circ$. As experimental results are not available at these plate positions, only the LES
 349 source results are used as reference. For $x_{TE} = 2D$, the noise levels show low sensitivity to
 350 the coherence parameter at angles in which edge-scattering is dominant. However, when the
 351 plate is positioned very close to the peak source ($x_{TE} = 6D$) and further downstream of the
 352 peak source ($x_{TE} = 8D$), noise results becomes more sensitive to the variation of L_c . Results
 353 from the unit coherence source, for instance, were about 6 dB/ St lower in comparison with
 354 the sources with finite L_c values for ($x_{TE} = 8D$). This is an interesting finding that suggest
 355 that the results become more sensitive to the coherence parameter as the trailing edge is
 356 moved downstream of the peak source. It is also possible to observe that the SPL variation
 357 decreases as the L_c value decreases.)

358 (Added: The variation of x_{TE} was useful to identify the effects of coherence when the plate
 359 is moved downstream of X_{max} . However, the results for $x_{TE} = 8D$, and even $x_{TE} = 6D$,
 360 should be observed with care as this configuration probably violates the hypothesis of low
 361 influence of the plate over the jet flow field. In this sense, these results may not reproduce
 362 well the aspects of the real phenomenon.)

363 (~~Deleted: Analysis with line source~~)

364 (~~Deleted: Indeed, the isolated jet case is very sensitive to source variations and the radial
 365 profiles carry some complexity regarding the range of length scales, for example. It should
 366 be thus much simpler to fit a line source with radially integrated LES data. For doing that,
 367 a line source was educed by considering radial compactness at low St . The derivation of the~~

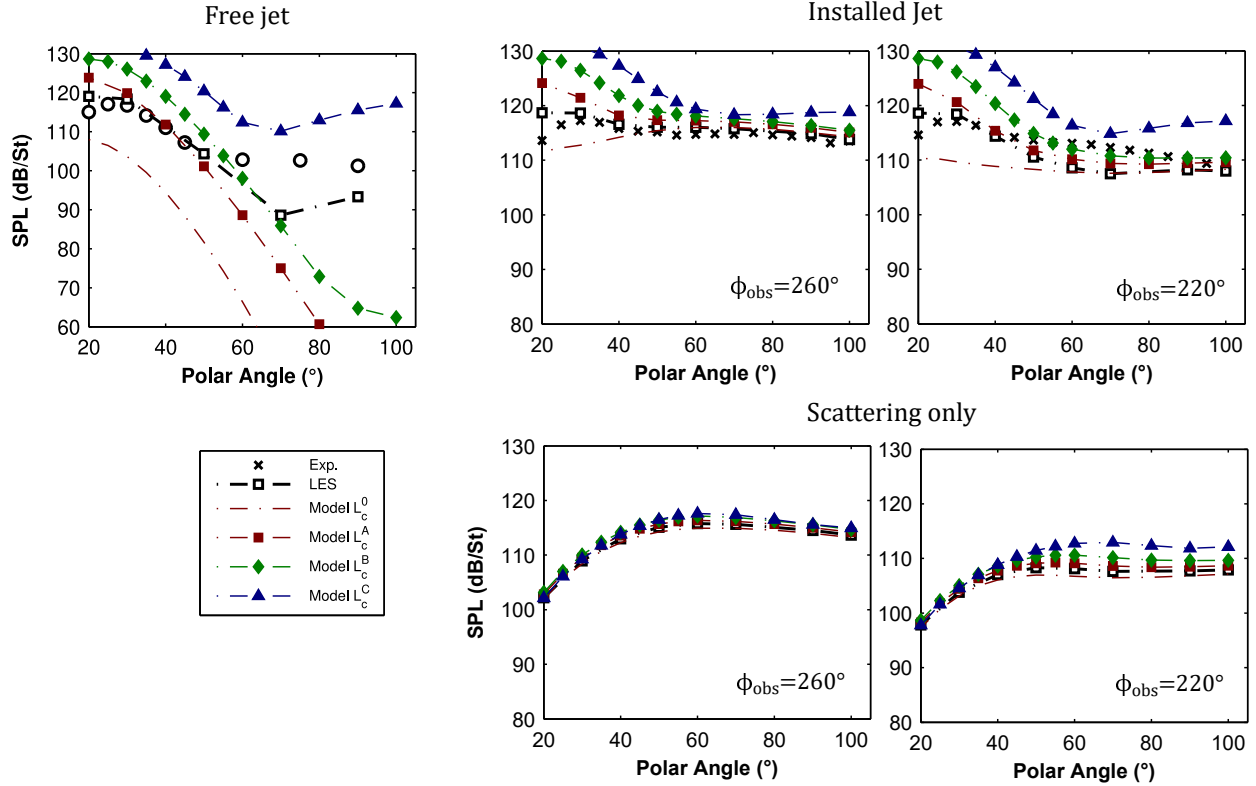


FIG. 8. (Color online) Model source results compared to the experiment and LES source for $St = 0.3$ with Free-field and tailored Green's function and varying L_c .

368 line source is described in section II E and the model shown in Eq. ???. The source parameters
 369 are obtained by using the double radial integral of the LES source and are summarized in
 370 table ???. This procedure is supposed to carry less uncertainties in the fitting process.)

371 (Deleted: Although the approximation sounds valid for the free jet, its application may
 372 be not accurate for the installed case, since the Green's function depends strongly on the
 373 distances between source and trailing edge, which varies azimuthally. Assuming radial
 374 compactness in this case probably leads to larger errors for the installed case. To reduce
 375 the effects of these simplifications, a cylindrical surface source, concentrated on the lipline

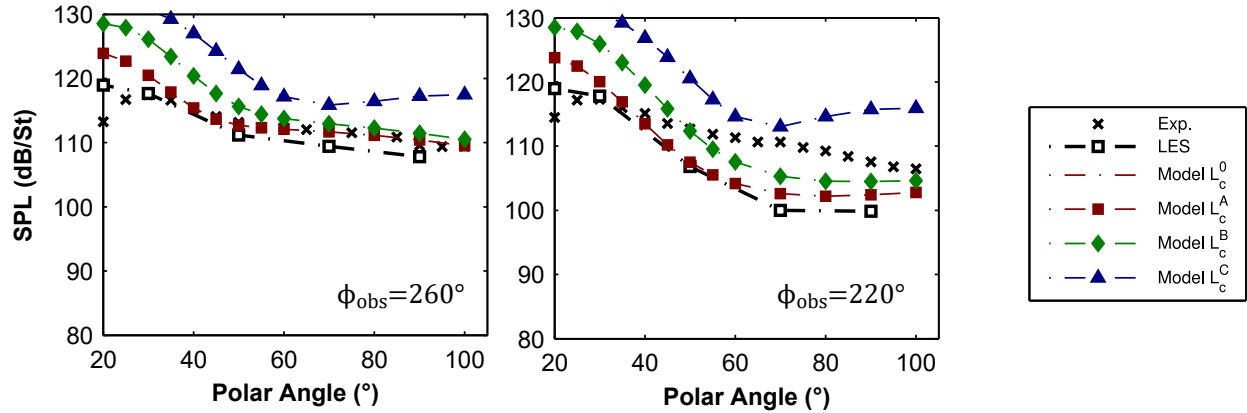


FIG. 9. (Color online) Model source results compared to the experiment and LES source for $St = 0.3$ with tailored Green's function for the plate at $r/D = 1.5$ and varying L_c .

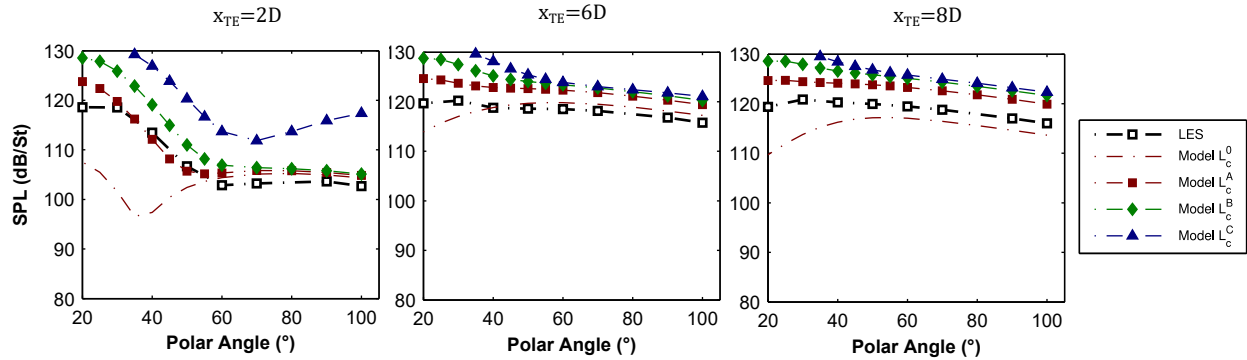


FIG. 10. (Color online) Model source results compared to the LES source for $St = 0.3$ with the plate at different axial positions and varying L_c . Observers at $\phi_{obs} = 260^\circ$.

376 is also used, as defined by Nogueira *et al.*¹². The same parameters used for the line source
 377 are used in the cylindrical surface approach.)

378 (Deleted: Some of the parameters in Table ?? changed significantly from those in Table I.

379 The axial position X_c appears more upstream for all St . The envelope length L_x now

380 decreases with St , a different trend from the two-dimensional fit. Higher values of k_n were

381 found for all St .)

382 ~~(Deleted: Acoustic results are show in Fig. ??(a) for $St = 0.2$, comparing the line and~~
 383 ~~cylindrical sources. For the isolated jet, results showed a slightly better agreement with~~
 384 ~~reference data in both the maximum amplitude and directivity when compared to the~~
 385 ~~previously used source model. However, noise levels are still overpredicted by about 4 dB.~~
 386 ~~Regarding installed jet cases (Fig. ??(d)), the results for $St = 0.2$ are in very good agreement~~
 387 ~~with the reference data, as well as the volumetric source. Minor differences can be noted~~
 388 ~~between the line and cylindrical surface sources, even for the installed case with plate at~~
 389 ~~$r/D = 1$.)~~

390 ~~(Deleted: Free jet results were also slightly improved for $St = 0.3$ (Fig. ?? (b)). For the~~
 391 ~~installed jet case (Fig. ?? (e)), the model results were about 4 dB higher than the reference~~
 392 ~~data. Besides possible inaccuracies in the fitting process, it is important to emphasize that~~
 393 ~~the use of the radially integrated data can lead to errors in the prediction of the jet-plate~~
 394 ~~noise.)~~

395 ~~(Deleted: Data for $St = 0.75$, depicted in Fig. ?? (c) reveals considerable differences~~
 396 ~~between the cylindrical surface and the linear sources. The noise levels were overpredicted~~
 397 ~~by about 4 — 5 dB by the line model and the cylindrical surface model could not correctly~~
 398 ~~reproduce the directivity trends.)~~

399 ~~(Deleted: Fig. ?? compares the radially integrated LES data with the fitted model sources~~
 400 ~~with reference point at X_{max} . We can now see that the model can reproduce the main~~
 401 ~~characteristics of the LES source in terms of PSD, CSD and coherence for the chosen St .~~
 402 ~~Indeed it becomes much simpler to fit line information with simple Gaussian functions in~~
 403 ~~comparison to the two-dimensional cases presented on the previous sections. The difficulties~~

404 ~~regarding the radial variation of the coherence lengthscale L_c , for instance, are overcome by~~
405 ~~compacting the coherence information on a line.)~~

406 ~~(Deleted: Fig. ?? shows that the asymmetric Gaussian function, with the obtained~~
407 ~~parameters, is suitable for modelling the PSD amplitudes. The amplitude and phases of~~
408 ~~the CSD were also well represented by the model at this position, as also shown in Fig. ??.~~
409 ~~It is important to note, however, that the shapes of both the CSD and coherence are not~~
410 ~~symmetric, especially for $St = 0.75$. In Fig. ??, for instance, the coherence shows a narrow~~
411 ~~peak, with rapid decay, followed by a much slower decay at the right side for $St = 0.75$.~~
412 ~~These features could not be well reproduced by the chosen Gaussian function.)~~

413 ~~(Deleted: Even though the asymmetric shapes of both the CSD and coherence could not~~
414 ~~be completely represented by the used functions, it is clear the information was enough for~~
415 ~~a good and fast prediction of the trailing-edge scattering noise. More complexity seems to~~
416 ~~be required for the isolated jet at higher St , both regarding the radial information and the~~
417 ~~analysis of the coherence function. This is outside the scope of the present study.)~~

418 V. CONCLUSION

419 A study of jet-plate interaction noise was conducted using numerical data as input for
420 wavepacket source models. A simplified source term was extracted from a numerical simu-
421 lation database and the corresponding acoustic field was obtained for both the free-jet, by
422 using the free-field Green's function, and for the installed jet by using a tailored function for
423 a semi-infinite plate. After analysing the main characteristics of the simplified source term,

424 the numerical data was used to adjust the parameters of simple source models. The noise
 425 prediction capabilities of such models were assessed for both isolated and installed jets.

426 The main features of the sound field for the isolated jet at low St and low polar angles
 427 could be obtained by considering only the linear part of the $T_{xx}(m = 0)$ source term extracted
 428 from the LES. Moreover, this term was show to be the main contributor to the jet-plate
 429 scattered field, confirming the observations from 10. Significant sensitivity to the window
 430 function used on the calculation of the source CSD was observed. In general, results using
 431 rectangular window were not desirable and presented large sensitivity to the block size, in
 432 comparison to the Hanning windows. This suggested high sensitivity of the acoustic analogy
 433 to errors in the signal processing.

434 ~~(Deleted: Two-and-one-dimensional)~~ Source models were built, ~~(Deleted: both)~~ by min-
 435 imising the squared error between the LES CSD and the proposed models. The sensitivity to
 436 the coherence length scales was analysed. By observing the CSD fields, the two-dimensional
 437 source approach could not correctly represent the characteristics of the source in every re-
 438 gion. That may be the main cause for the found deviations on the free-jet noise results.
 439 Anyhow, the installed jet noise ~~(Added: , for configuration in which trailing-edge scattering~~
 440 ~~is relevant,)~~ was seen to be much less sensitive to details in the modelled source.

441 ~~(Deleted: The use of simpler source models, such as line source adjusted with radially~~
 442 ~~integrated LES data, has proven to be more effective. This approach resulted in good~~
 443 ~~agreement with experimental data, a consequence of involving less uncertainties in the fitting~~
 444 ~~process. From the obtained results, we could observe that simplified models such as the ones~~

445 ~~used by 13 and 12 are able to correctly predict the noise levels for both installed and isolated~~
446 ~~jets, as long as they are parametrised with consistent source data.)~~

447 In summary, simple wavepacket models adjusted with flow field data, showed great ca-
448 pabilities to reproduce the noise level and directivity, specially for installed jets, with very
449 low computational effort; kinematic wave-packet sources may be useful for parametric stud-
450 ies of jet and wing placement, highlighting configurations with lower sound radiation. The
451 installed jet results were much less sensitive to fitting errors, specially to variations on the co-
452 herence parameters. In this way, modelling for installed jets becomes much simpler. (Added:
453 It is also important to mention that the analyses were limited to installed configurations in
454 which the jet flow is not significantly affected by the plate and so trailing-edge scattering
455 would be the main installation effect.)

456 ACKNOWLEDGMENTS

457 The LES study was performed at Cascade Technologies, with support from NAVAIR SBIR
458 project, under the supervision of Dr. John T. Spyropoulos. The main LES calculations were
459 carried out on DoD HPC systems in ERDC DSRC. The authors also acknowledge the support
460 from CNPq (National Council for Scientific and Technological Development - Brazil).

461 REFERENCES

462 ¹N. Curle, “The influence of solid boundaries upon aerodynamic sound,” Proceedings of
463 the Royal Society of London **231**, 505–517 (1955).

- 464 ²M. J. Lighthill, “On sound generated aerodynamically. I. general theory,” Proceedings of
465 the Royal Society of London. Series A. Mathematical and Physical Sciences **211**(1107),
466 564–587 (1952).
- 467 ³J. E. Ffowcs Williams and L. H. Hall, “Aerodynamic sound generation by turbulent flow
468 in the vicinity of a scattering half plane,” Journal of Fluid Mechanics **40**, 657–670 (1970).
- 469 ⁴P. Jordan and T. Colonius, “Wave packets and turbulent jet noise,” Annual Review of
470 Fluid Mechanics **45**(1), 173–195 (2013).
- 471 ⁵E. Mollo-Christensen, “Jet noise and shear flow instability seen from an experimenter’s
472 viewpoint,” Journal of Applied Mechanics **34**(1), 1–7 (1967).
- 473 ⁶S. C. Crow and F. H. Champagne, “Orderly structure in jet turbulence,” Journal of Fluid
474 Mechanics **48**, 547–591 (1971) doi: [10.1017/S0022112071001745](https://doi.org/10.1017/S0022112071001745).
- 475 ⁷C. E. Tinney and P. Jordan, “The near pressure field of coaxial subsonic jets,” Journal of
476 Fluid Mechanics **611**, 175–204 (2008) doi: [10.1017/S0022112008001833](https://doi.org/10.1017/S0022112008001833).
- 477 ⁸A. V. G. Cavalieri, P. Jordan, T. Colonius, and Y. Gervais, “Axisymmetric superdirectivity
478 in subsonic jets,” Journal of Fluid Mechanics **704**, 388–420 (2012) doi: [10.1017/jfm.
479 2012.247](https://doi.org/10.1017/jfm.2012.247).
- 480 ⁹A. V. G. Cavalieri, D. Rodríguez, P. Jordan, T. Colonius, and Y. Gervais, “Wavepackets
481 in the velocity field of turbulent jets,” Journal of Fluid Mechanics **730**, 559–592 (2013)
482 doi: [10.1017/jfm.2013.346](https://doi.org/10.1017/jfm.2013.346).
- 483 ¹⁰A. V. Cavalieri, P. Jordan, W. R. Wolf, and Y. Gervais, “Scattering of wavepackets by
484 a flat plate in the vicinity of a turbulent jet,” Journal of Sound and Vibration **333**(24),

485 6516–6531 (2014).

486 ¹¹S. Piantanida, V. Jaunet, J. Huber, W. R. Wolf, P. Jordan, and A. V. G. Cavalieri,
487 “Scattering of turbulent-jet wavepackets by a swept trailing edge,” *The Journal of the*
488 *Acoustical Society of America* **140**(6), 4350–4359 (2016) doi: [10.1121/1.4971425](https://doi.org/10.1121/1.4971425).

489 ¹²P. A. Nogueira, A. V. Cavalieri, and P. Jordan, “A model problem for sound radiation by
490 an installed jet,” *Journal of Sound and Vibration* **391**, 95 – 115 (2017) doi: [10.1016/j.](https://doi.org/10.1016/j.jsv.2016.12.015)
491 [jsv.2016.12.015](https://doi.org/10.1016/j.jsv.2016.12.015).

492 ¹³A. V. G. Cavalieri and A. Agarwal, “Coherence decay and its impact on sound radiation
493 by wavepackets,” *Journal of Fluid Mechanics* **748**, 399–415 (2014).

494 ¹⁴A. V. Cavalieri, P. Jordan, A. Agarwal, and Y. Gervais, “Jittering wave-packet models for
495 subsonic jet noise,” *Journal of Sound and Vibration* **330**, 4474 – 4492 (2011b).

496 ¹⁵Y. B. Baqui, A. Agarwal, A. V. G. Cavalieri, and S. Sinayoko, “A coherence-matched
497 linear source mechanism for subsonic jet noise,” *Journal of Fluid Mechanics* **776**, 235–267
498 (2015) doi: [10.1017/jfm.2015.322](https://doi.org/10.1017/jfm.2015.322).

499 ¹⁶D. Papamoschou, *Prediction of Jet Noise Shielding*, doi: [10.2514/6.2010-653](https://doi.org/10.2514/6.2010-653).

500 ¹⁷B. Lyu, A. P. Dowling, and I. Naqavi, “Prediction of installed jet noise,” *Journal of Fluid*
501 *Mechanics* **811**, 234–268 (2017) doi: [10.1017/jfm.2016.747](https://doi.org/10.1017/jfm.2016.747).

502 ¹⁸B. Lyu and A. P. Dowling, “Modelling installed jet noise due to the scattering of jet
503 instability waves by swept wings,” *Journal of Fluid Mechanics* **870**, 760–783 (2019) doi:
504 [10.1017/jfm.2019.268](https://doi.org/10.1017/jfm.2019.268).

- 505 ¹⁹G. A. Brès, P. Jordan, V. Jaunet, M. Le Rallic, A. V. G. Cavalieri, A. Towne, S. K.
506 Lele, T. Colonius, and O. T. Schmidt, “Importance of the nozzle-exit boundary-layer
507 state in subsonic turbulent jets,” *Journal of Fluid Mechanics* **851**, 83–124 (2018) doi:
508 [10.1017/jfm.2018.476](https://doi.org/10.1017/jfm.2018.476).
- 509 ²⁰P. Welch, “The use of fast fourier transform for the estimation of power spectra: A method
510 based on time averaging over short, modified periodograms,” *IEEE Transactions on Audio
511 and Electroacoustics* **15**(2), 70–73 (1967) doi: [10.1109/TAU.1967.1161901](https://doi.org/10.1109/TAU.1967.1161901).
- 512 ²¹S. C. Crow, “Acoustic gain of a turbulent jet *Phys. Soc. Meeting, Univ. Colorado, Boulder*,”
513 paper IE, vol. 6. (1972).
- 514 ²²D. Crighton, “Basic principles of aerodynamic noise generation,” *Progress in Aerospace
515 Sciences* **16**(1), 31 – 96 (1975) doi: [10.1016/0376-0421\(75\)90010-X](https://doi.org/10.1016/0376-0421(75)90010-X).
- 516 ²³A. Michalke and H. Fuchs, “On turbulence and noise of an axisymmetric shear flow,” *J.
517 Fluid Mech.* **70**, 179 (1975) doi: [10.1017/S0022112075001966](https://doi.org/10.1017/S0022112075001966).
- 518 ²⁴D. Juvé, M. Sunyach, and G. Comte-Bellot, “Filtered azimuthal correlations in the acoustic
519 far field of a subsonic jet,” *AIAA Journal* **17**(1), 112–113 (1979) doi: [10.2514/3.61076](https://doi.org/10.2514/3.61076).
- 520 ²⁵D. J. Bodony and S. K. Lele, “Low-frequency sound sources in high-speed turbulent jets,”
521 *Journal of Fluid Mechanics* **617**, 231–253 (2008) doi: [10.1017/S0022112008004096](https://doi.org/10.1017/S0022112008004096).
- 522 ²⁶C. J. Mead and P. J. R. Strange, “Under-wing installation effects on jet noise at side-
523 line,” in *4th AIAA/CEAS Aeroacoustics Conference*, AIAA 98-2207, American Institute
524 of Aeronautics and Astronautics (1998).

- 525 ²⁷J. Lawrence, “Aeroacoustic interactions of installed subsonic round jets,” PhD thesis,
 526 University of Southampton, Faculty of Engineering and the Environment, 2014.
- 527 ²⁸J. A. Nelder and R. Mead, “A simplex method for function minimization,” The Computer
 528 Journal **7**(4), 308 (1965) doi: [10.1093/comjnl/7.4.308](https://doi.org/10.1093/comjnl/7.4.308).

TABLE I. Values of the resulting source parameters from the CSD fits. Non-dimensional values.

St	A	X_c	L_x	α	L_r	k_h	L_c	Δ
0.2	1.18×10^3	9.32	5.92	0	0.17	1.67	3.95	0.64
0.3	0.31×10^3	3.26	9.45	-5.06	0.16	2.6	3.00	0.63
0.75	0.07×10^3	1.77	7.91	-22.8	0.11	6.01	3.31	0.84

List of Changes

Added: **at the region dominated by trailing-edge scattering**, on page 2, line 10.